NUMERICAL AND EXPERIMENTAL ANALYSES OF THE STRESS FIELD AHEAD OF FATIGUE CRACKS IN LASER-TREATED AA2198-T851

Cauê P. Carvalho[*1], João P. Pascon[1], Milton S. F. Lima[2], Carlos A. R. P. Baptista[1]

[1] Engineering School of Lorena, University of São Paulo (EEL/USP), Lorena/SP, Brazil ([*]email: caue.pc@usp.br)
[2] Institute of Advanced Studies, Department of Aerospace Science and Technology (IEAv/DCTA), São José dos Campos/SP, Brazil

Abstract: Laser heating treatment (LHT) is a residual-stress-based approach exhibiting successful results in reducing fatigue crack propagation rates in laboratory specimens. Although its effect is usually related to the original residual stress field, it is known that cyclic loading and crack growth can cause relaxation and redistribution of residual stresses. In this work, M(T) specimens made of 2.0 mm thick AA2198-T851 alloy sheets with L-T and T-L crack orientations were treated with a fibre laser (power 200 W, displacement speed 1 mm/s) to produce two heating lines ahead of each crack front on one of each specimens' face. Constant-amplitude loading tests were conducted on treated and untreated specimens at a zero-to-tension condition (R = 0). In addition, electrical resistance strain gauges bonded 4 mm away from the notch tip along the crack path were employed to measure the deformation behaviour ahead of the approaching crack tip. A numerical model was developed for the stress-strain state ahead of the crack, including plane stress condition, linear elastic response, the anisotropic Gurson-Tvergaard-Needleman (GTN) yield criterion coupled with damage, associative plastic flow rule and nonlinear isotropic hardening Swift model. The mesh refinement was concentrated around the crack path direction from the notch tip until the specimen's edge. The experimental results showed significant fatigue crack growth (FCG) retardation experienced by the laser-treated specimens; this effect was more pronounced in the L-T orientation. Numerical simulations could depict the stress field distribution in the treated specimen. Numerical simulations of damage increment under monotonic loading were adopted for a preliminary evaluation of the effect of LHT on the strain behaviour of the specimens.

Keywords: Laser heating; Fatigue crack growth; Numerical analyses; AA2198-T851.

INTRODUCTION

Beyond the mere objective of achieving cost reduction, sustainability has emerged as a paramount preoccupation within the industrial sector. For instance, the aviation industry, being one of the largest consumers of transportation fuel worldwide, contributes substantially to the global emissions of greenhouse gases (GHG). Given the exponential increase in air traffic, doubling every fifteen years, prominent corporations in the aircraft industry, such as Airbus, Boeing, and General Electric have

acknowledged the indispensability of embracing sustainable practices as a strategic business opportunity [1,2].

One of the main issues regarding fuel reduction and lower operational cost is the aircraft weight. Therefore, the aerospace industry is always demanding the development of lighter aluminium alloys, the main metal employed in this sector [3,4]. The significance of incorporating lithium in aluminium alloys dates back to the Cold War era when the first generation of the Al-Li system was developed. The potential of this alloy system can be highlighted by the fact that the addition of the alkaline metal leads to a density reduction of 3% for every 1% increase in its concentration, followed by an increase in rigidity and fatigue crack growth (FCG) resistance [3,5]. Currently, in its third generation, the Al-Li system can be found on the shelves, and companies such as Airbus and the Chinese COMAC employ these alloys in the fuselage skin of their modern aircraft. For instance, the AA2198, which was used in this work, is a contemporary Al-Li alloy, intended to replace conventional 2xxx ones, such as 2024 and 2524 [1]. This material was evaluated as a fuselage skin candidate for the Airbus A350, before the project considered predominantly utilising composite materials. However, the alloy is currently employed in the Airbus A220, former CSeries from the Canadian Bombardier.

On the matter of enhancing fatigue life, residual-stress-based techniques such as shot peening, cold expansion and laser shock peening are well known. Another surface treatment for this subject is the laser heating treatment (LHT), which had the potential of retarding FCG in aeronautical aluminium alloys emphasized in the past decade [7-10]. The technique consists of local heating, arising from the interaction between the laser beam and the material in a continuous line, followed by fast cooling. Similar to weld behaviour, the heated area associated with the laser incidence promotes tensile residual stresses. However, in the surrounding area, a compressive residual stress field is formed. In light of that, laser heating lines are applied perpendicularly to the crack path, to achieve better efficiency of this field, once it is responsible for a crack closure. In that way, a decrease in the FCG rate is observed, enhancing the component's life. LHT requires a laser power source, but in contrast with LSP, which demands pulsed wave laser equipment, the first only needs a continuous one. That being said, LHT has the potential for cost savings, due to a less expensive equipment necessity, also demanding a weaker power source, which reduces the environmental impact of the technique, compared with LSP.

Schnubel et al. [7] evaluated the effect of LHT in an aluminium alloy, for instance, the AA2198-T8, the one employed in the present work. The authors employed C(T)100 specimens orientated in the T-L direction, out of a 5.0 mm sheet. The treatment involved local heating with a defocused laser beam, to avoid melting. Furthermore, a thin layer of silicon carbide was deposited on the irradiated surface to assure uniform absorption of the laser light for all specimens. The outcome of this observation revealed a remarkable 100% enhancement in the FCG life. Subsequently, Groth et al. [9] examined the effect of LHT on M(T)200 specimens of AA2024-T3 with a thickness of 2 mm. The study aimed to investigate the effect of different configurations of the laser line, on specimens with geometry that more closely resembled those of aircraft structures. The authors observed a positive effect of both continuous and dashed lines on FCG, with two heating lines deemed optimal for the technique's application. However, care must be taken to maintain an appropriate distance between the second line and the first to avoid compromising the compressive residual stresses generated by the latter.

The authors of the current manuscript have previously investigated the impact of LHT on aluminium alloys [10]. In that particular work, TL-oriented C(T)50 specimens of AA2198-T851 with a thickness of 2 mm were subjected to two heating lines. Before the application of the Yb: fibre laser beam, a thin black graphite layer was employed. The authors evaluated two scanning speeds (1 mm/s and 10 mm/s), maintaining a single 200 W power level, with a 2 mm laser spot-defocused beam. The main contribution of that study was the analysis of different loading ratios (R), as the majority of literature on this topic has focused on the 0.1 R-ratio, while the authors also included an investigation of R = 0.5. Both scanning speeds exhibited a degree of FCG retardation, but the slower treatment was particularly noteworthy. Concerning the R-ratio analysis, it was observed that the treatment presented a comparatively negligible impact in tests involving higher R-ratios, whereas more pronounced outcomes were observed in R = 0.1 tests. Furthermore, different R-ratios from the ones already employed should be studied.

Previous investigations have employed numerical techniques to study the effects of LHT. For example, Schnubel and Hubel [11] conducted a thermal-mechanical analysis of the 2198-T8 alloy to determine the residual stresses induced by the technique. They subsequently simulated a crack and calculated the associated stress intensity factor, later using an empirical model to evaluate the crack propagation rate (da/dN). Results indicated that the laser heating effectively delayed the fatigue crack growth. Similarly, Groth et al. [8] also employed FEA to evaluate the effect of both continuous and dashed lines in M(T)200 specimens of AA2024-T3. However, despite these previous studies, there remains an opportunity for new investigations of LHT about relaxation and/or redistribution of the residual stress field. In this context, the present work employs another numerical methodology to evaluate the effects of LHT.

The anisotropic Gurson-Tvergaard-Needleman (GTN) yield criterion coupled with damage was originally introduced by Gurson [12] and subsequently improved by Tvergaard [13] and Tvergaard and Needleman [14]. This model is based on a plastification criterion that incorporates the influence of mean stress, as well as ductile damage, measured as the volumetric percentage of discontinuities on the material. The current study intended to utilize the GTN model to examine M(T)50 AA2198-T851 specimens that were subjected to treatment with two sets of heating lines, one on each front of the crack path. In addition, the study aims to conduct a first step in the analysis of the redistribution and/or relaxation of stresses to some extent. To do so, electrical resistance strain gauges were bonded right next to the first heating line. This analysis could inform the strain behaviour in this area as the crack advanced. The study was conducted for different crack sizes in both L-T and T-L directions, with a null R-ratio. Notably, no prior research has explored this R-ratio value for LHT, despite its significance in the aeronautical field. Furthermore, numerical analysis was employed in order to advance the discussion on this matter, but considering here a monotonic loading.

EXPERIMENTAL

Laser heating process

The present study conducted experimental investigations on a 2 mm thick sheet of AA2198-T851, the constituent elements of which are provided in Table 1. The alloy exhibited yield and ultimate tensile stresses of 438.9 MPa and 480 MPa, respectively, along with Young's modulus of 69 GPa and a Poisson's ratio of 0.35. M(T)50 specimens with both L-T and T-L orientations were employed in the study and subsequently subjected to LHT.

Table 1: AA2198-T851 composition in weight percent (Al as balance).

Elements	*Cu*	*Li*	*Si*	*Fe*	*Mg*	*Mn*	*Ti*	*Ag*	*Zr*	*Zn*
% wt.	3.68	1.01	0.03	0.08	0.305	-	0.027	-	0.12	0.01

Laser heating was performed using an IPG Photonics Yb: fibre laser, model YLR-2000, with a maximum power output of 2kW. The specimen displacement was controlled by a three-axis CNC table, where the X and Y-axes were responsible for controlling the position and scanning speed of the technique, while the Z-axis controlled the laser focus, and consequently the spot size diameter. To achieve a 2 mm focal diameter on the specimen surface, the optical head was positioned 12.2 mm above the focal length. A power level of 200 W was maintained at a scanning speed of 1 mm/s, as defined in previous studies [10]. Figure 1 illustrates a sketch of the specimens, along with their corresponding heating lines. It is worth noting that Figure 1 also depicts a sketch of the non-treated specimens. The specimens were treated with two pairs of laser heating lines, one in each of the crack fronts. The lines closer to the crack tip were spaced 22 mm apart from each other, while the more distanced ones were separated by 30 mm. It is worth noting that the configuration of heating lines was arranged symmetrically in the specimens. To prevent excessive heating due to the slow laser scanning speed, the heating lines were 100 mm long, as presented in Figure 1. In order to do so, the laser began scanning the sample at a distance of 36 mm from the top edge, stopping at a similar position at the bottom to centralize the lines.

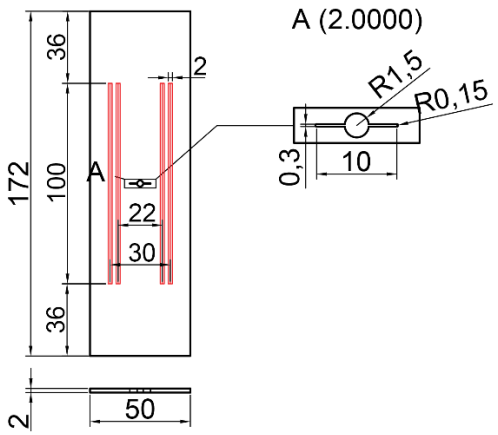

Figure 1: Sketch of the investigated M(T)50 specimen with detail of the notch. Marked in red are the laser heating lines.

Fatigue crack growth tests

Fatigue crack growth tests were conducted with constant load amplitude under force control using an MTS 810 servo-hydraulic machine. The tests were in accordance with the ASTM E647-15e1 standard and carried out in laboratory air at room temperature. Prior to the experiment, pre-cracking was performed, letting the pre-crack grow about 1 mm of each notch tip and ensuring that the final maximum load was less than the maximum load of the test, for which the data were obtained. Zero-to-tension tests were performed at a constant frequency of 5 Hz with a sinusoidal loading waveform. As for the crack length monitoring, the compliance method was used during the tests. The subsequent crack growth rate was later calculated using the secant method.

During the FCG tests, strain measurements were performed right next to the first heating line. To do so, half-bridge HBM LY43-0.6/120 linear strain gauges were bonded 9 mm ahead of the specimen theoretical centre, on each side of the crack front. The 120 Ω resistance strain gauges with the k-gauge factor of 1.73 had their centre positioned on the crack propagation line. Data acquisition was carried out with a QuantumX MX840A universal amplifier, assisted by the catmanEasy software. The acquisition frequency was 1200 Hz, allowing over 200 points per loading cycle. Data were acquired every 10,000 cycles, reducing this interval as fluctuations were sensed. The mean strain was obtained, using data from strain gauges of both sides of the crack front, this strain value was used in the following steps. The nominal stress-versus-time curves were simulated such that their minima coincided with the strain gauge data, in an effort to obtain hysteresis loops from the test results. By comparing the acquisition cycle to the FCG curves, it was possible to evaluate the hysteresis loops data for different crack sizes in each specimen. Therefore, a comparison between treated and non-treated conditions was possible for both specimen orientations.

NUMERICAL ANALYSIS

The effect of the laser treatment was numerically evaluated with a finite element program. To this end, a thermoviscoplastic GTN ductile damage model has been implemented in a computer code using 2D linear-order triangular finite elements. The isotropic constitutive model selected accounts for linear elastic response, plane stress conditions, strain and strain-rate hardening, porosity-induced softening, void growth and nucleation and thermal effects, such as plastic work heating, thermal softening and heat diffusion. Further details regarding the constitutive framework can be found, for instance, in the work of Pascon and Waisman [16]. The material coefficients are presented in Table 2 and have been extracted from the works of Zhang et al. [17] and Yildiz and Yilmaz [18]. The strain hardening is described by the Swift law based on the level of the equivalent plastic strain κ. The relationship between the equivalent stress σ_{VM} and the yield stress level σ_Y is defined by the GTN modification in the classical von Mises yield criterion, including the mean stress p and the adjusting parameters q_1 and q_2, as well

as the level of ductile damage measured by the void volume fraction f. Associative plasticity is assumed for the plastic strain rate $\dot{\varepsilon}_p$. Regarding the damage evolution, the nucleation contribution ($\dot{f}_{nuc}$) based on the plastic strain is added to the growth term ($\dot{f}_{gr}$). The strain effect is accounted for by means of the modified viscoplastic Litonski model applied for the equivalent plastic strain rate $\dot{\kappa}$, together with thermal softening (s). The effects of temperature are considered in the isotropic linear dilatation model and in the heat equation ($\dot{T}$), including plastic work converted into heat (χW_p) and Fourier's thermal conduction ($C_T \nabla^2 T$).

Table 2 - Material coefficients employed in the numerical simulations.

Model	*Parameters*	*Unit*	*Equation*
Swift	K = 423.63 $\varepsilon_0 = 0.00380602$ n = 0.0549	MPa - -	$h = K(\varepsilon_0 + \kappa)^n$
Yield criterion	q_1 = 1.5 q_2 = 1.0 f_0 = 0.01 f_F = 0.04	- - - -	$\sigma_{VM} - \sqrt{1 + (q_1 f)^2 - 2q_1 f cosh\left(\frac{3q_2 p}{2\sigma_Y}\right)}\sigma_Y \leq 0$
Void nucleation	f_N = 0.001 s_N = 0.3 ε_N = 0.1	- - -	$\dot{f} = \dot{f}_{gr} + \dot{f}_{nuc} \qquad \dot{f}_{gr} = (1-f)tr(\dot{\varepsilon}_p)$ $\dot{f}_{nuc} = \frac{f_N}{s_N\sqrt{2\pi}} exp\left[-\frac{1}{2}\left(\frac{\kappa - \varepsilon_N}{s_N}\right)^2\right]$
Viscoplasticity	g_0 = 0.00167 m = 14	1/s	$\dot{\kappa} = g_0\left(\frac{\sigma_Y}{h\, s}\right)^m$
Thermal softening	δ = 0.5 T_0 = 295 k_T = 1000	- K K	$s = 1 - \delta\left[exp\left(\frac{T - T_0}{k_T}\right) - 1\right]$
Thermal dilatation	α = 0.000023	1/K	$\dot{\varepsilon}_t = \alpha \Delta T$
Thermal coefficients	$\hat{c} = 920$ $\chi = 0.9$ $\rho = 2700$ $C_T = 204$	J/kg K - kg/m^3 W/m K	$\rho \hat{c} \dot{T} = \chi W_p - C_T \nabla^2 T$

In the finite element approximation, a kinematical framework considering finite deformations and possibly high strain levels is employed. Additional information about the triangular element, the large strain decomposition and the solution of the resultant nonlinear system of equations is available in [19], among others. Due the symmetry of the specimen regarding the vertical plane, only one half of the specimen has been discretized, resulting in a mesh with 440 nodes and 822 finite elements.

The present numerical study involved the analysis of both AR and LHT conditions. In the first case, only a simple mechanical simulation under displacement control was performed. For the LHT condition, in turn, a two-step procedure was necessary: a thermal analysis followed by a mechanical simulation. The first step was carried out by means of increasing the temperature according to a specified heating profile and decreasing it to the initial values in the sequence. Following the temperature solution presented by Bergheau, Robin and Boitout [20], a double-layer exponential heating was employed, as shown in Figure 2. The peak value of the temperature is about 500˚C, which is close to the level presented by Schnubel and Huber [11] for a moving heat source. Based on that profile, the temperature is imposed at the nodes of the mesh and the program determines the resultant strains and stresses. In the second step, the information obtained at the end of the heating/cooling stage is employed as an input for the mechanical simulation of the specimen under LHT condition. In all the simulations, the computer code determines numerically the nodal values of displacements, temperature and damage, as well as the local values at the elements of the yield stress and plastic strains.

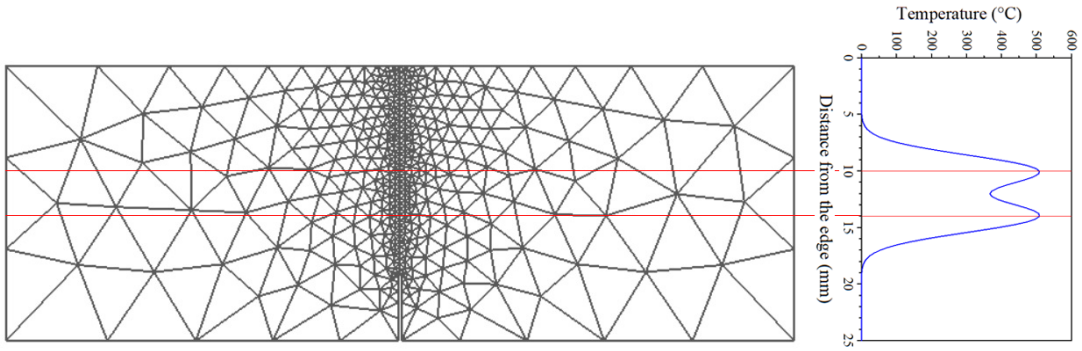

Figure 2: Discretization adopted together with the temperature distribution. The peaks at the graph correspond to the position of the laser lines ($x = 10\ mm$ and $x = 14\ mm$).

RESULTS AND DISCUSSION

Fatigue crack growth analysis

Figure 3 depicts the data on crack length versus the number of cycles (a versus N) for both LT and TL specimens in the as-received (AR) and laser heat-treated (LHT) conditions. First of all, it is worth noting that no significant difference in life is observed between the different orientations in the AR conditions. TL-AR specimen presented a 9% higher number of cycles to fail than the LT-AR one, which could be related to the scattering behaviour in FCG. Furthermore, LT-oriented specimens are reported in the literature as exhibiting a deviation in the fatigue crack path [7], which would reflect in longer lives for this orientation. Once the opposite was observed in the current tests, this indicates an influence of only the scatter factor. However, it is important to point out the deviation effect in LT specimens, considering that LHT can amplify this behaviour with the compressive residual stress field that arises from the treatment. This field presents a challenge for the crack to follow its natural perpendicular-to-loading path, resulting in the search for a new orientation in which to propagate, enhanced by the natural tendency of the LT orientation.

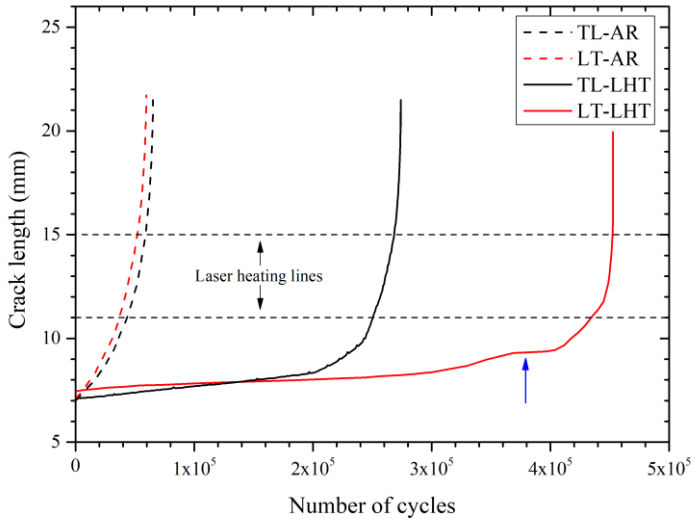

Figure 3: Crack length versus the number of cycles' curves of L-T and T-L specimens, for both as-received (AR) and laser heat-treated (LHT) conditions.

The laser treatment demonstrated remarkable performance in both orientations, with particularly noteworthy results in the LT direction. The TL-LHT specimen exhibited a 320% increase in lifespan compared to its non-treated counterpart, while the LT-LHT specimen displayed an outstanding increase of over 650%. The higher life observed in LT orientation reinforces the previous discussion regarding

the effect of orientation. However, upon comparison with the TL-LHT data, a discernible deviation in the trend of the curve can be noticed in the LT-THL specimen between 350,000 and 400,000 cycles, as indicated by the blue arrow in Figure 3. This phenomenon may be attributed to the differential deceleration of one crack front relative to the other, suggesting a higher difficulty in overcoming the compressive field. In order to expand this discussion, Figure 4 is provided, illustrating the da/dN versus ΔK curves for all four specimens.

Prior to the previous discussion, it is worth mentioning that Figure 4 highlights that the impact of laser treatment is only pronounced within a region preceding the first heating line. Subsequent to this point, LHT specimens follow the same trend as that observed in AR specimens, after an increase in the FCG rate. Particularly in the LT-LHT specimen, this behaviour is extrapolated, since after the first heating line, the FCG rate of the specimen is higher than the AR condition, ultimately leading to the final fracture. Nonetheless, the initial retardation is adequate to cause a noteworthy effect on the lifespan of specimens, as previously discussed.

Both TL-LHT and LT-LHT initiated the experiments with FCG rates lower than 10^{-8} m/cycle. The former demonstrates an ascendant asymptotic trend from 10^{-9} m/cycle up to 10^{-8} m/cycle. Conversely, the latter exhibits descending asymptotic trend in FCG rates from 10^{-8} m/cycle to approximately 10^{-9} m/cycle. Despite the disparity in behaviour, both specimens' performances would suffice to infer a comparable lifespan between them. However, the blue arrow in Figure 4 points out a second decreasing trend in FCG rate in the LT-LHT specimen, which is consistent with that observed in Figure 3. In light of this, it is evident that this second decrease is responsible for the difference in the treated lifespans of both specimens. Given that no noteworthy difference in the AR conditions is observed and that after the first heating line, the TL-LHT specimen exhibits a similar response, the behaviour of the LT-LHT specimen may not be directly influenced by the sample orientation, but rather due to this second delay in the fatigue crack. Further discussion will be presented in the strain measurement analysis.

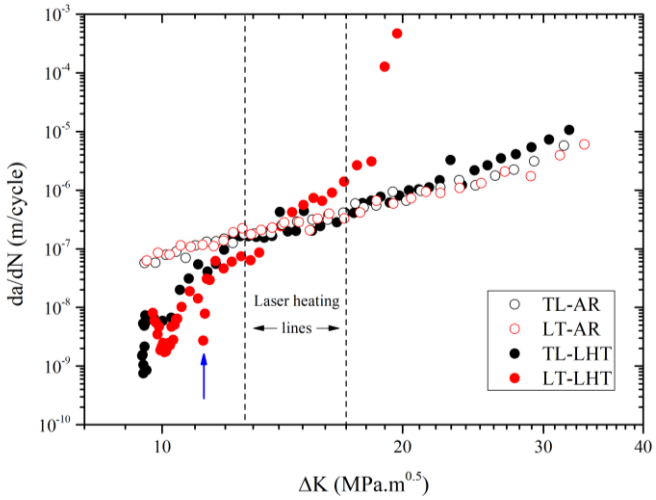

Figure 4: da/dN versus ΔK of cycles curves of L-T and T-L specimens, for both as-received (AR) and laser heat treated (LHT) conditions.

Strain gauge data analysis

This section presents data from the strain measurements performed during FCG tests. Figure 5 displays the collected data, which compares AR with LHT conditions. Specifically, Figure 5a shows an analysis of TL-orientated specimens, while Figure 5b depicts LT specimens. Hysteresis loops were obtained for different crack sizes (7.00 mm, 7.60 mm, 7.90 mm, and 8.00 mm). It is worth noting that the data collection process took into consideration the variable number of cycles, and some approximations were employed to convert data into crack length using the a versus N curves. In addition, for the LT-LHT specimen with a 7.00 mm crack, the data were not collected, hence instead of it, 7.50 mm crack data was used as the first hysteresis loop of this specimen.

In the subsequent discussion, only the maximum strain-nominal stress pair will be considered, as the laser effect is expected to be more prominent when the crack is fully open. The minimum pair may be affected by crack-closing effects due to the zero-to-stress loading nature, which could interfere with the analysis. In this study, the strain gauge was utilised to measure the strain response of the material subjected to the nominal stress of the test.

As the crack tip represents a site of stress concentration, it generates a concentrated strain field. While the crack growth proceeds, the strain associated with the crack tip will influence the data measurements. Consequently, the strain gauge data demonstrate an increase in the strain measures for larger cracks, as summarized in Figure 5. The impact of the treatment effect is once again emphasized as the maximum strain measured in LHT samples is comparatively lower than that of AR specimen. The compressive static field induced by laser lines, when superimposed with the test loadings, functions to reduce the normal stress ahead of the crack tip [10]. In this case, the K_{max} is reduced, which consequently leads to a decrease in the associated measured strain. This is the reason why smaller cracks exhibit similar maximum strains between the AR and LHT conditions, while the difference becomes more noticeable with increasing crack size.

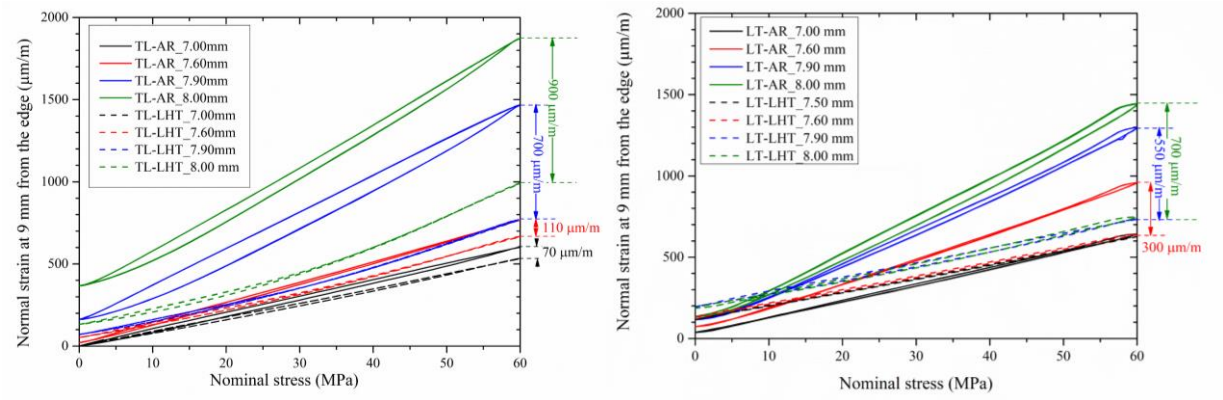

(a) (b)

Figure 5: Hysteresis loops evaluating AR and THL conditions for different crack sizes, in which (a) represents TL specimens; and (b) LT ones.

In the TL specimens with a crack size of 7.00 mm, the difference in maximum strain between AR and LHT conditions is approximately 70 µm/m. This small difference is due to the distance of the crack tip.in relation to the strain gauge, becoming a challenge to measure the strain field associated with this site. However, as the crack size increases to its maximum detected value (8.00 mm), the difference in maximum strain between the two conditions increases up to 900 µm/m, which is 12 times higher than the initial value. A similar trend is observed in the LT specimens, but as the LT-THL sample lacks 7.00 mm data, some inferences must be made with 7.5 mm data employed instead. A superposition of this data with the LT-AR data for 7.00 mm is evident, and no more than 100 µm/m difference is observed for the subsequent data set (7.90 mm). Therefore, it is clear that 7.00 mm LT-LHT data should be smaller than the LT-AR data, but with a difference no greater than 100 µm/m, similar to the TL specimens. As crack size increases in both AR and LHT conditions, the difference in maximum strain gradually increases in LT specimens, reaching a final difference of 700 µm/m.

In summary, Figure 5 provides additional evidence that LHT has a beneficial effect in retarding fatigue crack growth. Moreover, this dataset provides insights into the strain behaviour during crack propagation, which could give information about the relaxation and redistribution of the stress field induced by the treatment. Also, further discussions are necessary concerning specimen orientation. Accordingly, Figure 6 repositions the data presented in Figure 5 to allow for a comparison of different orientations. Figure 6a depicts the results for the AR specimens, while Figure 6b illustrates the data for the LHT samples.

Figure 6, in contrast to the findings of Figure 5, does not demonstrate a gradual increase in the dissimilarity between the compared conditions. The AR specimens show a decrease in the difference as the cracks grow from 7.60 to 7.90 mm. Similarly, in the LHT specimens, no noticeable difference is observed until an 8.00 mm crack is reached. It could be argued that the last detected crack length presents a higher difference than the previously observed ones. However, this may be related to the previously discussed approximations or some degree of asymmetry between the crack fronts, which could affect the mean strain values. Among all specimens, a substantial difference is detected between 7.90 to 8.00 mm cracks, which is higher than the previously examined ones. This observation aligns with the earlier argument. Additionally, as previously discussed, the LHT samples in the a versus N curves were interpreted as being more affected by the orientation of the specimen than AR specimens. Conversely, the 8.00 mm crack difference in AR was more prominent, with a value of 450 μm/m against 250 μm/m for the LHT specimens. Hence, no significant difference was observed in the orientation of the specimen. It is more probable that approximations and asymmetry, such as the one indicated by the blue arrow in Figures 3 and 4, have an effect on the small differences observed rather than the orientation itself.

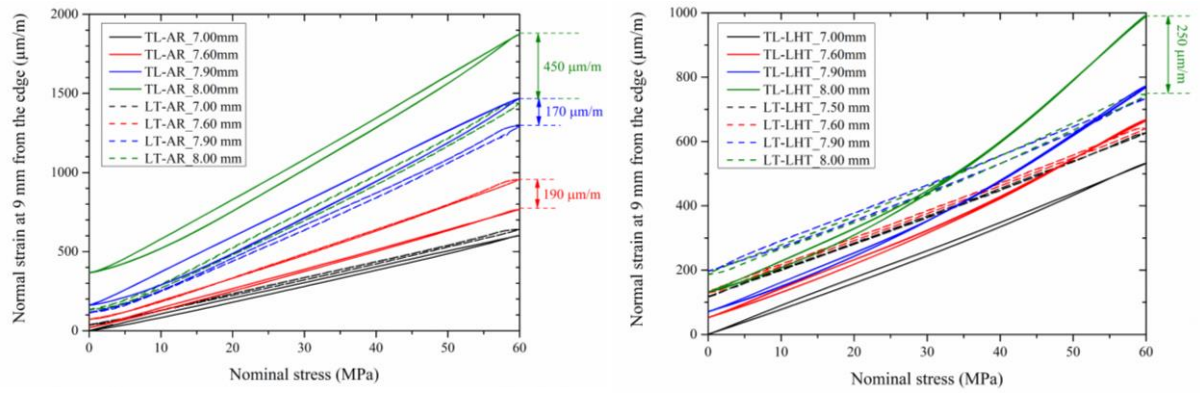

(a) (b)

Figure 6: Hysteresis loops evaluating TL and LT orientations for different crack sizes, in which (a) AR conditions; and (b) LHT ones.

Numerical analysis

Considering the LHT situation, the temperature profile depicted in Figure 2 is incrementally applied along 100 steps and then returns to the initial temperature of 295 K, also in 100 steps. The resultant distribution of the normal stress along the loading direction at the end of the heating/cooling stage is provided in Figure 7a, in which one can observe high levels of residual stresses. Such levels are comparable with the stress distribution obtained in the work of Schnubel and Huber [11] using a moving heat source. As expected of the LHT technique, tensile residual stresses are located in the treated area, surrounded by a compressive residual stress field. The LHT area presented a tensile residual stress of around 190 MPa, on the other hand, the adjacent area exhibit a compressive field around 180 MPa. This behaviour reinforces the beneficial effect of the treatment, as already discussed in the authors' previous work [10]. In addition, one can highlight the large level of compression around the notch tip, around 548 MPa.

In the mechanical analysis for both AR and LHT conditions, the prescribed vertical displacement is applied uniformly at the upper edge of the specimen up to a value of 0.36 mm along 0.1 second, which corresponds to a nominal vertical strain of 0.5% and a nominal strain rate of 0.5 /s. In this case, 1000 steps are employed to achieve convergence. The vertical displacements of the bottom face are restricted and, due to the symmetry condition, the horizontal displacements of the right face are prevented.

The effect of the laser heating is numerically investigated by means of the stress evolution at the notch tip and the strain evolution at a specific point, located 9 mm from the right edge or 3 mm from the notch tip (considering the initial crack length of 6 mm). In Figure 7b, it is clear that the laser heating (LHT) delays the evolution of the stress at the notch, which is desirable in order to increase the resistance to

cracking. Despite the monotonic nature of the loading, it reinforces the delayed crack growth presented in the experimental data.

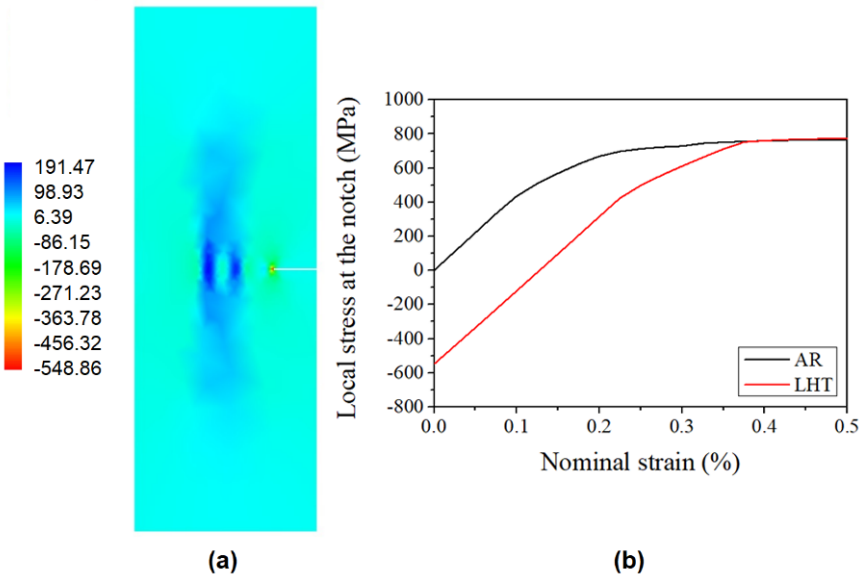

Figure 7: Normal stresses (MPa) along the loading direction: (a) distribution of residual stresses at the end of the heating/cooling stage (LHT condition); (b) evolution of stress the notch tip for both AR and LHT conditions.

Regarding the strain levels, the laser heating also delays the evolution of local strain at the selected point, which implies that a higher level of nominal strain is needed to obtain a specific value of local strain, see Figure 8. Although the present numerical analysis is monotonic, the differences in terms of strain levels are similar to the experimental results depicted in Figures 5 and 6 considering cyclic loading. Considering that this region is similar to the strain gauge position, it is worth mentioning that some degree of strain is observed before the application of loading, which is not taken into account in the experimental section, once the strain gauge is bonded after the LHT. Beyond that, the present analysis is a first step in the matter of the relaxation study of residual stresses. Further development of the model should allow a comparison between the strain gauge and numerical data.

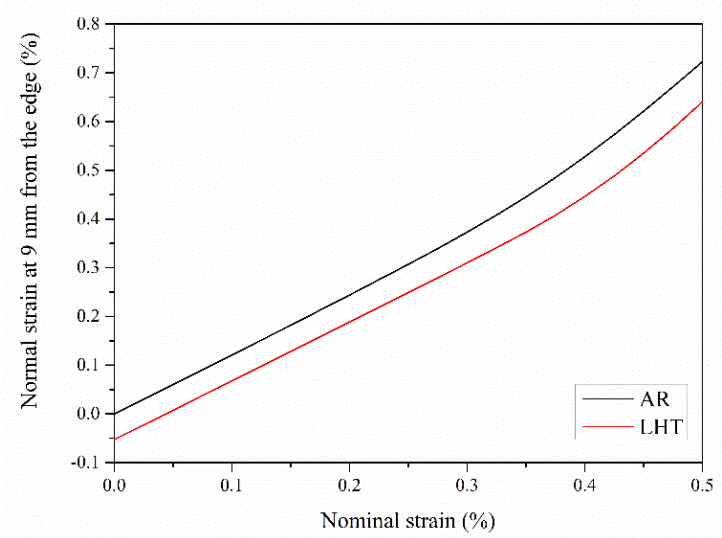

Figure 8: Evolution of the normal strain along the loading direction at the point located 9 mm from the right edge of the specimen.

CONCLUSION

The current work showed the influence of LHT in FCG tests of AA2198-T851 M(T) specimens, being successful in enhancing the fatigue life. Both LT and TL specimens exhibited an increase in lifespan greater than 300%, with the effect in the first direction being more noticeable. However, strain gauge data indicated no clear influence of the direction itself, suggesting another cause of this behaviour, such as a more prominent deflection in one of the crack fronts, as reinforced by the da/dN versus ΔK data. Also, the derivative curves support the idea that LHT effect on FCG is more pronounced before the crack front achieves the first heating line. Once the crack advances this point, treated specimens follow the same trend as the AR ones. This observation is due to the fact that tensile residual stresses are present in the treated lines, but compressive ones are exhibited in the surroundings, as shown in the numerical analysis section. Furthermore, numerical analysis indicated that the notch tip presented the greatest compressive values, around 550 MPa. This region displayed a decay in the compressive stress when the specimen is subjected to a monotonic nominal strain, during the simulation, however delaying the evolution of the stress when compared to the AR condition. A similar analysis was conducted on a point in the theoretical crack path located 9 mm from the specimen's edge, being both analyses a first glance at the LHT behaviour during loading application. Beyond them, the strain gauge data provided initial information regarding the redistribution of residual stresses and highlighted how the LHT causes the normal strain values to decrease for the same crack sizes, compared to the AR condition. Further development of the numerical model should be able to correlate experimental data and numerical analysis.

FUNDING/ACKNOWLEDGEMENTS

This research was funded by the São Paulo State Research Support Foundation (FAPESP), grant number 2018/16438-9. C.P.C. acknowledges the Coordination of Superior Level Staff Improvement (CAPES) and C.A.R.P.B. acknowledges the National Council for Scientific and Technological Development (CNPq) for the research grants.

REFERENCES

[1] Hallstedt, S. I., Bertoni, M. and Isaksson, O. (2015), *Journal of Cleaner Production*, vol. 108, p. 169-182.
[2] Gialos, A. A., Zeimpekis V., Alexopoulos N. D., Kashaev N., Riekehr S. and Karanika A. (2018) *Journal of Cleaner Production*, vol. 176, p. 785-799.
[3] Alexopoulos N. D., Migklis E., Stylianos, A and Myriounis D. P. (2013), *International Journal of Fatigue*, vol. 56, p. 95-105.
[4] Tavares, S. M. O., dos Santos J. F. and de Castro, P. M. S. T. (2013), *Theoretical and Applied Fracture Mechanics*, vol. 65, p. 8-13.
[5] Rioja R. J., Liu, J. (2012), *Metallurgical and Materials Transactions* A, vol. 43A, p. 3325
[6] Zhao, F., Naik, G., Zhang, L. (2009). In: Manufacturing Science and Engineering Conference, Proceedings of the ASME 2009 International, vol. 43611, pp. 97-105, West Lafayette.
[7] Schnubel, D., Horstmann, M., Ventzke V., Riekehr, S., Staron, P., Fischer, T. and Huber, N. (2012), *Materials Science and Engineering A*, vol. 546, p. 8-14.
[8] Groth A., Horstmann M., Kashaev N. and Huber N. (2015), *Procedia Engineering*, vol. 114, p. 271-276.
[9] Cunha, M. C. and Lima, M. S. F. (2017), *Surface & coatings technology*, vol 326, p. 244-249.
[10] Carvalho, C. P., Lima, M. S. F., Pastoukhov, V. and Baptista, C. A. R. P. (2021), *Metals*, vol. 11, p. 2034.
[11] Schnubel, D. and Huber, N. (2012), *Computational Materials Science*, vol. 65, p. 461-469.
[12] Gurson, A. L. (1977), *Journal of Engineering Materials and Technology*, vol. 99, p. 2-15.
[13] Tvergaard V. (1982), *International Journal of Fracture*, vol. 18, p. 237-252.
[14] Tvergaard V. and Needleman, A. (1984), *Acta Metallurgica*, vol. 32, p. 237-252.

[15] Sérgio, E. R, Antunes, F. V., Neto, D. M. and Borges, M. F. (2021), *Metals*, vol. 11, n. 8, p 1183.
[16] Pascon, J.P. and Waisman, H. (2021), *Mechanics of Materials*, vol. 153, p. 103701.
[17] Zhang, Q., Zhang, C., Lin, J., Zhao, G., Chen, L. and Zhang, H. (2019), *Materials Science and Engineering: A*, vol. 742, p. 773-787.
[18] Yildiz, R.A. and Yilmaz, S. (2020), *European Journal of Mechanics-A/Solids*, vol. 83, p. 104040.
[19] Pascon, J.P. (2019), *International Journal of Advanced Structural Engineering*, vol. 11, p. 331-350.
[20] Bergheau, J.M., Robin, V. and Boitout, F. (2000), *Journal-Shanghai Jiaotong University*, vol. 5, p. 114-122.